DESIGN OF REAR WING OF AN ELECTRIC RACE CAR

Steffan Johan Kirk – S170816
Carl-Emil Grøn Christensen – S170817
Department of Mechanical Engineering, Technical University of Denmark

Supervisor:
Jens Walther
Department of Mechanical Engineering, Technical University of Denmark

June 2018

Acknowledgements

We would like to thank our supervisors Jens Walther and Robert Mikkelsen, who allowed us to learn intricate details about our own personal project. A special thanks to everyone on the team of Vermilion Racing, who in less than a year managed to take a dream and make it reality. Vermilion Racing is going to compete at the Silverstone race track the 10th of July, where all of our ideas and designs are going to be tested to the limit.

Thanks to Rasmus Himborg from Philips Lighting Denmark, for helping us machine a 1/4 scale wing used in the wind tunnel tests.

Thanks to Bo Tranberg for assisting with graphical setup of the report and making sure our figures are beautiful.

Thanks to Nicolai Boertmann and Daniel Rasmussen for the help building the composite wings.

Thanks to DTU Skylab, and especially Martin Meister, Rasmus Bruun, Ralle Malone and Tonja Kramer for always having the time to help us when things looked most dire.

Lastly, a thank to Nenad Mijatovic. Nenad is the overall supervisor for Vermilion Racing and is a significant reason we recently became a DTU Blue Dot project - a highly prestigious title that will ensure that the team will survive for many years to come.

GRANBY FOAM
fitting unique demands

POWERFINN
PART OF MICROPOWER GROUP

ekwb

HobbyKing.com

DTU Skylab
- where it begins

NORDEA FONDEN
Vi støtter gode liv

Farnell

DTU
Technical University
of Denmark

KLEE

SKF

alumeco
TO BE NO.1

SIEMENS | Fonden

mouser.com

cft

AV-CABLES.dk

AVON TYRES

OZ RACING

COMLINE
AUTO PARTS

GUNNAR AASKOV MOTORSPORT

IWAKI

Tranes Fond

Ensinger

RIAS

LiTHIUM BALANCE
BATTERY MANAGEMENT SYSTEMS

Karl Pedersen & Hustru Fond

Mogens Balslevs Fond

OTTO MØNSTEDS FOND

Abstract

Race cars wooo! Formula studee3333nt

Contents

1

Introduction

Vermilion Racing is a newly started Electric race car team building their first vehicle: The Eevee [1]. The teams' purpose is competing against other Universities at the Silverstone race track from the 11^{th} to the 16^{th}. As members of the team, the purpose of this report is to document the design process of the rear wing of the first car, the Eevee, and provide an aerodynamic package documenting drag and downforce.

Aerodynamics is a major decider in racing today. Cornering, not top speed is the deciding factor amongst the teams, and aerodynamics is the key. Drag, lift and side force are the three cornerstones to vehicle aerodynamics. A car's ability to handle depends on the grip of the tyres, and downforce directly increases grip by increasing the downwards load on the tyres without adding a weight penalty. Additionally, drag directly decreases the speed of a vehicle by increasing air resistance, but is of less importance as the car's in this class have far more accelerative power than the tyres can handle [2]. Designing the bodyworks of Eevee is therefore a dance of downforce.

This bachelor thesis attempts to lay down the ground work for designing, optimizing and manufacturing the car's rear wing. Our advisor, Jens Honore Walther, proposed simulating the wing geometry in order to both cheapen and quicken the optimization process, but also gain insight into how flow in front of the rear wing affects lift performance. The purpose of the numerical simulations are ultimately to create an easily producable wing in a very short timespan, that produces ample amounts of negative lift for the time spent in production.

FiXme Note: write about what has been done prior

As this is the first year the team building a car, time and money for production is sparse. To ensure the simulated optimizations are true, a wind tunnel test is performed on a down-scaled wing using Flow Similarity theory. The measurements are compared with the results from a computational fluid dynamics simulation performed in Star-CCM+ to verify the preciseness of the simulations. Based on this, the size, x- and y-distance between the multi-element wings, angle of attack and height relative to the chassis is then optimized for maximum downforce. The multi-element wing is taken from theoretical abstraction to reality with a physical design of the wing. The position, deflection and dimensions of the wing is thoroughly described by the rules of the Formula Student competition, guiding the final design process. In the final chapter, theories regarding strength of sandwich structured composites and carbon fiber molding are handled, in order to descibe the production choices made. Finally, the end result is discussed and possible improvements to the wing and mounting system is listed.

Measurements and tests have been carried out at the DTU Wind laboratory's Red wind tunnel with the help of our supervisor Robert Flemming Mikkelsen the 19^{th} of June.

The entire project is publicly available on `https://github.com/carlegroen/bachelor_project_racecar_aero`, where all work files, data, various notes and CAD drawings can be found. The Formula Student team at DTU: Vermilion Racing can be followed on `fb.com/FSDTU`.

1.1 Design Philosophy

Designing a car with hundreds, if not thousands different factors is incredibly difficult. Therefore, analyzing which things matters and which don't is crucial to the teams' success. First, the deadline for finishing the wing is soon. This sets a limit on the complexity of the wing's dimensions. Secondly, this is the first iteration of the car, thus no decision can be based on prior experience, and optimization has to wait for the next iteration. Finally, the finances of the car is tight. This forces us to go with a low-cost solution. We therefore have to go for a simple, low cost wing, basing the design solely on litterature and experience other teams have done.

The wing has to have as low weight as possible, in order to ensure optimum acceleration of the car. Thereto, drag has to be kept low, but the effect from drag is near negligible, which will be explained in section 2.1. Lastly, we have to maximize the downforce provided by the wing, but also ensure that the center of pressure is kept as constant as possible. If the frontwing, undertray and rear wing's downforce don't scale equally with speed, the center of pressure will move during acceleration. This will make the car's handling unpredictable, and potentially limit the driver's confidence in the car.

2

Aerodynamic Effects on Vehicle Performance

The first argument to the importance of aerodynamics is based around two facts: The fact that drag is neglible in regards to the Formula Student vehicle's top speed on straights, and the fact that aerodynamically increasing the vehicle's *effective* mass due to downforce increases tyre grip, which in turn allows for higher cornering velocities.

The second part of this chapter covers the importance of centering the effective mass increase due to aerodynamic devices close to the center of gravity – otherwise handling characteristics becomes a function of velocity.

2.1 Drag Effects on Straights

First, let's explain what makes a car fast, and what parameters we can change to improve the speed of our car.. The car's acceleration can be described by Newton's second law as:

FiXme Note: introduce a figure with drag and lift to show what's going on

FiXme Note: stort D eller lille d i ligningen?

$$\sum F_x = m\ddot{x} = F \tag{2.1}$$

Where the sum of forces in the x-direction (the direction of travel) can be expressed as the force already pertained by the vehicle, minus the drag force:

$$F - C_D \left(\frac{1}{2} \rho \dot{x}^2 A \right) = m\ddot{x} \tag{2.2}$$

Figure 2.1: Frontal area of the car with a dummy wing inserted into the CAD model, in order to get an estimate of the drag coefficient C_D.

Where C_D is the drag coefficient of the vehicle, ρ is the density of the fluid it moves in and A is frontal area of the vehicle. Assuming we're moving at a steady speed, the acceleration is 0, hence

$$F = C_D \left(\frac{1}{2} \rho \dot{x}^2 A \right) \tag{2.3}$$

As we were interested in the speed of the car, let's solve for the velocity. The force is given by $F = \frac{P}{\dot{x}}$, where P is the power of the car, which gives:

$$\dot{x} = \left(\frac{2P}{C_D (\rho A)} \right)^{\frac{1}{3}} \tag{2.4}$$

This is assuming we're traveling at terminal velocity – that is, the point where the Driving Force = Friction Force. The terminal velocity of the racer is then easily calculated, as the competition restricts the maximum amount of power to 80 kW, and the frontal area of the car is approximated from the CAD drawing seen in figure 2.1.

FiXme Note: fix calculation to use 0.99 instead of 1.2

FiXme Note: missing radiators

$$\dot{x}_{\max} = \left(\frac{2 \cdot 80\,\mathrm{kW}}{0.85\,(1.225\,\mathrm{kg\,m^{-3}}\;1.2\,\mathrm{m^2})} \right)^{\frac{1}{3}} = 50\,\mathrm{m\,s^{-1}} = 181.4\,\mathrm{km\,h^{-1}} \tag{2.5}$$

however, given the ruleset a forecasted maximum of 110 km h^{-1} allows a much larger drag coefficient C_D:

$$C_D = \frac{2P}{\dot{x}^3 (\rho A)} = \frac{2 \cdot 80\,\mathrm{kW}}{(120\,\mathrm{km\,h^{-1}})^3\,(1.225\,\mathrm{kg\,m^{-3}}\;1.2\,\mathrm{m^2})} = 2.82 \tag{2.6}$$

FiXme Note: insert source

Thus, the car's top speed will only be limited by a drag factor > 2.82, which is far above the drag introduced by the aerodynamic devices.

From this derivation, it is clear that the car's abilities at maximum speeds far exceed the requirement of the track. Therefore, the next step is to improve cornering speeds which depend strongly on the tyre's grip on the surface of the road [2].

2.1.1 Downforce Effects on Cornering

Shown before, drag does not limit the car's performance on straights. During cornering, drag is not an issue either, but the grip of the tyres limits the maximum velocity before the vehicle loses traction due to the centripetal force which is given by: [3]

$$F_{\text{centripetal}} = \frac{m\dot{x}^2}{r} \tag{2.7}$$

where r is the distance to the center of the cornering circle. The frictional force the car exerts due to downforce and tyre grip is given by:

$$F_{\text{friction}} = \mu F_{\text{normal}} \tag{2.8}$$

where the normal force is given by both the weight and (negative) lift of the car, which serves as an effective mass increase:

$$F_{\text{friction}} = \mu \left(mg + \frac{1}{2}\rho C_L A \dot{x}^2 \right) \tag{2.9}$$

The vehicle will lose traction when the frictional force is less than the centripetal force.

$$\frac{m\dot{x}^2}{r} > \mu \left(mg + \frac{1}{2}\rho C_L A \dot{x}^2 \right) \tag{2.10}$$

Giving the maximum velocity for a given corner radius before the car skids out:

$$\Rightarrow \dot{x} < \left(\frac{2\mu mgr}{m - \mu C_L \rho r A} \right)^{\frac{1}{2}} \tag{2.11}$$

Again, the forecasted variation in radii of corners is prescribed by the rules to be between 3 m to 50 m [4]. Plotting this for various C_L values between 1.5 to 2.6 [5], assuming $m = 300\,\text{kg}$, $\mu = 1.5$ [6] and $A = 0.99\,\text{m}^2$ as previously used. The result can be seen in figure 2.2.

2.1.2 Load Distribution

The scope of this thesis is not to incorperate a full aerodynamic package, but a quick overview of load distribution is essential to understanding the behaviour of the car.

The effective mass added from negative lift depends on the lift coefficient. It is evident that different items on the car carry different lift coefficients,

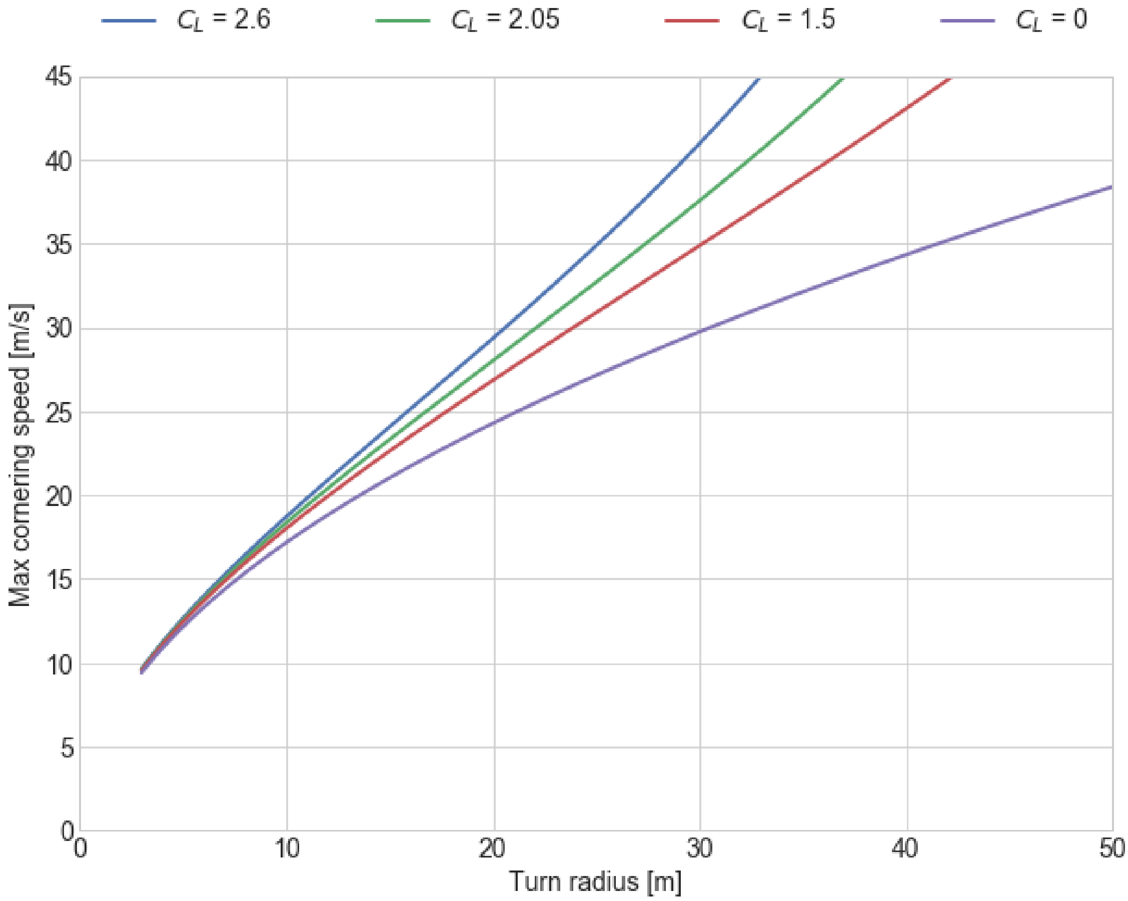

Figure 2.2: Cornering speed as a function of turn radius for various lift coefficients.

thus making the lifting forces over the cars length a function of relative speed. For the unexperienced driver, this is not easily managed as handling characteristics change with velocity. Therefore, it is desirable to have the aerodynamic center of pressure close to the car's center of gravity, in order to have similar handling at all velocities. While this is not handled in this thesis, it is ideal for future iterations and essential for a full aerodynamical package.

3

Airfoils and Inverted Wings

FiXme Note: fix the dot x to u for wind velocities

Achieving a large negative lift coefficient C_L can be done in many ways. Inspecting race cars throughout the years show that airfoils have been used as early as 1966 when Jim Hall attached a rear wing to his Chaparral 2E [7]. Since then, the inverted wings have been a staple in the racing industry with various three dimensional geometries affecting the overall performance even further.

This chapter covers the pressure distribution of various airfoils, the selection criterions of the competition, three dimensional geometrical effects and the tools of the optimization trade.

3.1 Airfoil theory

An airfoil is the 2-dimensional cross section of a wing, that is defining of the wing's lifting characteristics. It is important to know the nomenclature: The leading edge is the most forward point of the wing, the trailing edge is the most rearward point of the wing. Camber is how much the wing the wing *bends*.

FiXme Note: consider figure here

When an airfoil moves in a fluid, the streamlines of the particles move as seen in figure 3.1. The streamline stops at the stagnation point, which is usually the leading edge. The other can be divided into two categories, as the flow can only go to two places: The *suction surface* and the *pressure surface*.

The suction surface is the surface where the flow accelerates to high velocities and the pressure drops. This can be seen on the top part of figure 3.1, where the corresponding pressure distribution can be seen below as

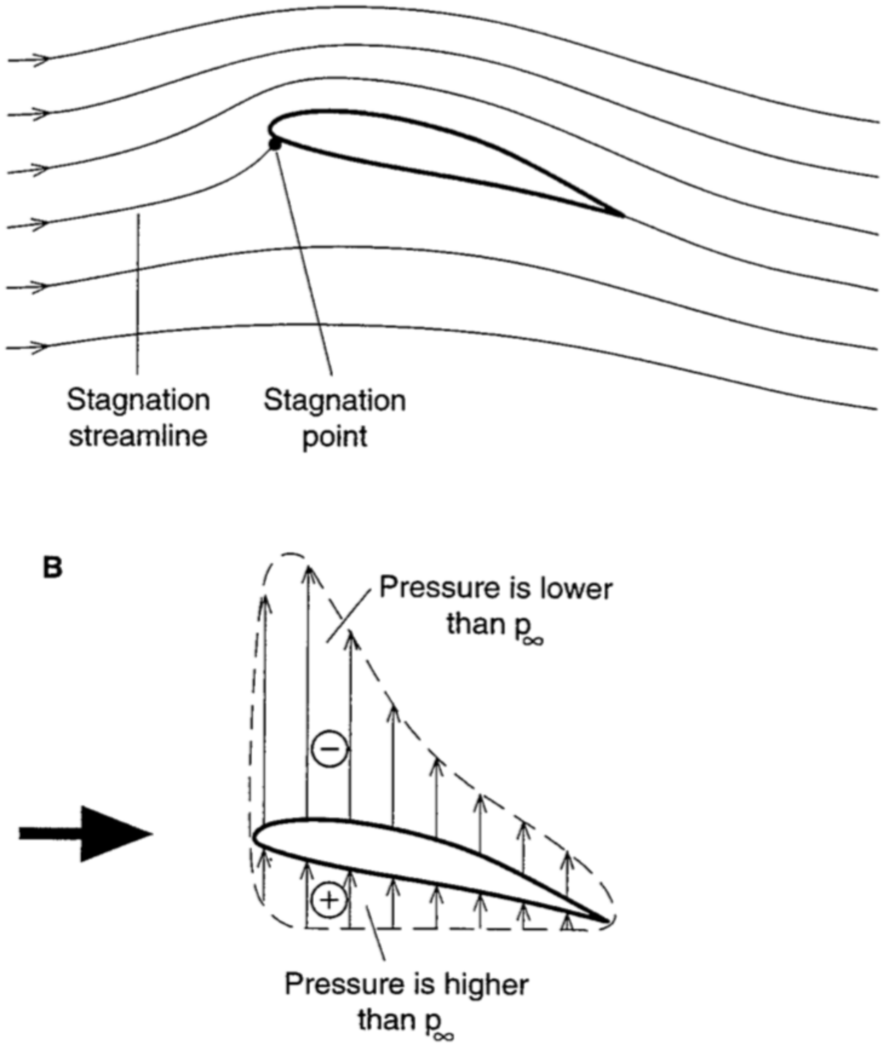

Figure 3.1: A figure showing the streamlines around a slightly cambered airfoil, along with its pressure distribution below.

the (-) part. A peak of very low pressure can be found near the leading edge, which is often called the suction peak.

The pressure surface is the surface where the flow decellerates to lower velocities and the pressure increases. This is the bottom part of 3.1, which provides a much lower force from the pressure than the suction side.

The resulting changes in pressure forces the wing upwards, creating lift. It it important to note, that the suction side contributes considerably more to lift in most cases [2].

3.1.1 Airfoil Lift and How to Increase it

Increasing the lifting capabilities of an airfoil can be done in several ways.

First, the angle of attack of air airfoil usually increases lifting characteristics of a wing, until reaching a certain threshold where it falls off. An airfoil carries its lifting abilities usually while flow is attached - that is, where the streamlines follow the shape of the airfoil. If the flow separates from the surface of the airfoil, the lift behaviour becomes unpredictable. This effect is called *stalling*.

There are two types of stalling: Leading edge separation which are quite abrupt and greatly decreases lift, and trailing edge separation, which gradually reduces the lift. These are called a hard and soft stall, respectively. Thus, a soft stall is prefered in racing, as a hard stall will instantly change the car's handling abilities.

Secondly, another way of changing the lift is by creating an effective change in angle of attack: Changing the wing's camber. The trailing edge of an airfoil's camberline is the largest contributor to lift. By changing the camber geometry, the lift can be changed greatly, and the largest increase is found in the trailing edge region. This is why the introduction of flaps is prominent in both aircraft and race car wings.

Lastly, the thickness of the airfoil affects lift up to a certain point, and the optimum thickness is about 12% of the camber length. For the interested ready, reference [2] explores this further.

3.1.2 Lift and Drag Coefficient

The lift coefficient is a dimensionless coefficient that relates the lift generated to the fluid the airfoil moves in, the velocity of the fluid and the reference area. This coefficient is defined as:

$$C_l \equiv \frac{l}{\frac{1}{2}\rho {u_\infty}^2 c} \tag{3.1}$$

Where L is the lift per unit width, ρ is the density of the fluid, $\dot{x}_\infty$ is the velocity of the surrounding fluid and c is the chord length. For a specific wing, that is, where an airfoil has a physical extension, the lift coefficient is defined as:

$$C_L \equiv \frac{L}{\frac{1}{2}\rho {u_\infty}^2 A} \tag{3.2}$$

Where L is the total lift force, and A is the surface area. For a wing with both camber and angle of attack, C_L is found by the following formula:

$$C_L = C_{L_\alpha}(\alpha + \alpha_{L_0}) \tag{3.3}$$

where α is the lift per angle of attack in radians, α_{L_0} is the airfoil's camber, which acts as a additional angle of attack effect, also in radians. C_{L_α} is given by:

$$C_{L_\alpha} = \frac{2\pi}{1 + \frac{2}{AR}} \tag{3.4}$$

[8]

Like lift, a dimensionless drag coefficient exist, that describes how drag is generated in a similar fashion:

$$C_d \equiv \frac{2F_d}{\rho u^2 A} \tag{3.5}$$

Where F_d is the drag force - the component of the force that is parallel with the flow velocity [9]. The induced drag created by the lifting force must also be added in order to find the total drag coefficient:

$$C_D = C_d + C_{d_{\text{induced}}} \tag{3.6}$$

where $C_{d_{\text{induced}}}$ is given by:

$$C_{d_{\text{induced}}} = \frac{C_L^2}{\epsilon \pi AR} \tag{3.7}$$

FiXme Note: something about Navier Stokes equations.

[10] The derivation and explanation hereof is found in the section below.

3.1.3 Aspect Ratio and End Plates

An important identifyer when describing an actual finite wing is, apart from chord length and airfoil design, the width. The definition used for describing the physical span is called Aspect Ratio, and for a rectangular wing is:

$$AR_{\text{actual}} = \frac{b}{c} \tag{3.8}$$

Where b is the width of the wing and c is the chord length.

The effect of having a finite length is very important in race aerodynamics. As pressure is lowered and increased on the different sides, air is going to travel around the edge of the wing in a rolling motion. This creates a vortex, which is shown in figure 3.2. The phenomenon is called tip vortices,

Figure 3.2: The trailing tip vortex is clearly seen to the right. Thanks to the NASA's Wake Vortex Study for the photo [11].

and the magnitude of the vortex is proportional to the lift coefficient of the wing. The area these vortices cover is very large and for wings with a small span will greatly reduces the lifting powers.

These vortices are created by an effect called *downwash* when talking aeroplanes. As the wing bends the air slightly downwards, it creates an opposite force due to Newton's second law which is lift. However, the sheet of air that passes over the length of the wing has a downward velocity component and will thus force air in that direction. This presses other air out of the way, allowing air above it to rush downwards to fill the gap. The same phenomenom is what happens at the edge of the wing, and again is what is shown in figure 3.2. When the wing *bends* the airflow downward, drag is induced. While drag is almost negligible in our case, it is never wanted [12]. For an elliptical wing, the induced drag coefficient is given by:

$$C_{d_{\text{induced}}} = \frac{C_L^2}{\epsilon \pi \text{Æ}} \tag{3.9}$$

Where $\epsilon = 1$ for an ellipse, and generally $\epsilon < 1$ for anything else. For a rectangular wing, $\epsilon = 0.7$ [10].

A way to combat this phenomenon is the addition of end plates. End plates adds a virtual additional length by adding a physical wall between the low- and high pressure surfaces. The vortices that usually go around the wing and reduce lift is severely hindered. A corrected aspect ratio can be found for wings with side plates as:

$$\mathit{AR} = \mathit{AR}_{\text{actual}} \left(1 + 1.9 \frac{h}{b} \right) \tag{3.10}$$

where h is the height of the end plate, and b is the width of the wing as in equation 3.8 [2]. The addition of end plates gives an increased aspect ratio. Inserting this back into 3.4 shows that end plates yields an increase in lift.

3.1.4 Multiple Elements and Maximum Downforce

As mentioned before, in order to increase downforce on a wing (made of a predefined airfoil) there is two options: Increasing the width of the wing, or increasing the camber. As the width is fixed by regulations, the camber has to be varied. Increasing camber usually causes flow separation, but by splitting the airfoil into multiple elements, this can be circumvented while gaining effective airfoil camber. The camber attained by using multiple elements is usually much higher than with a single element, and letting the high pressure from the first element transition to the low pressure zone of the secondary element results in a favorable interaction between the two elements .

FiXme Note: is it this way that it works?

The lift coefficient can be seen as a function of angle of attack in figure 3.3. Notice how the angle of attack can be increased before stalling occurs and lift increases. A leading airfoil (also called a *slat*) will extend the angle of attack even further, but will not increase the lift curve [2].

3.2 Wing Parameters

The previous sections describe which parameters can be varied in order to attain better aerodynamical properties, such as higher lift, robustness towards stall and protection against trailing tip vortices. Improving a wing has several optimization parameters, and below is a table of how these are going to be handled in the following sections:

Parameter	Effect	Optimization Technique
Thickness	Usually predefined by airfoil	N/A
Angle of Attack	Changes lift characteristics	Finding the optimum angle of attack
Camber	Usually predefined by airfoil	Adding additional Elements
Position between elements	Changes lift characteristics	Optimizing x, y position between elements
Size	Sizes directly increases lift	Finding the maximum allowed size by regulations

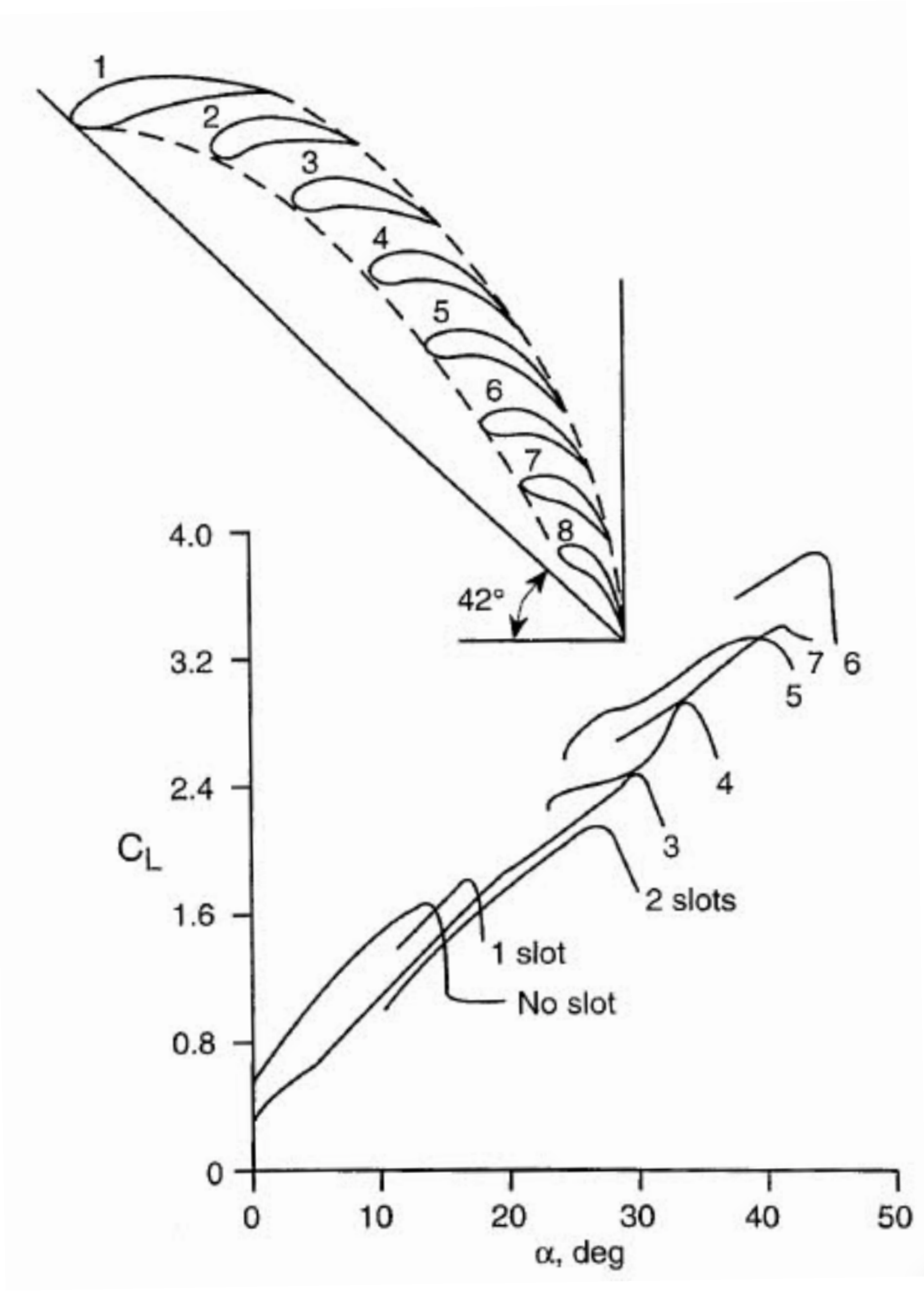

Figure 3.3: Lift coefficient as a function of effective angle of attack. The *No slot* line corresponds to a single element wing, and the *1 slot* corresponds to a double element wing. Figure taken from [2].

4

Concept Design

The following contains the conceptual design of a rear wing based on the previous chapters. First, a walkthrough of different airfoil profiles and their benefits is followed by selection of one particular. Second, analyzing the amount of elements the wing should consists of with regards to production time and ease of construction. Third, the dimensional requirements outlined by the competition rules are given, and finally, a Product Design Specifiation (PDS) is set up to make sure that the design solution addresses all the problems it attempts to solve. Based on the PDS, an initial design is proposed, followed by a section describing the various possible methods of optimization.

4.1 Comparison of Airfoils

Finding a fitting airfoil requires deep investigation of airfoil databases and articles. The requirements for this airfoil according to the PDS is a really high lift wing, operating at large ranges of Reynolds numbers, where the highest (according to track regulations) is around:

$$\mathrm{Re} = \frac{uL}{\nu} = \frac{30.56\,\mathrm{m\,s^{-1}}0.6\,\mathrm{m}}{1.491 \times 10^{-5}\,\mathrm{m^2\,s^{-1}}} \approx 1.2 \times 10^6 \tag{4.1}$$

to around:

$$\mathrm{Re} = 3 \times 10^5 \text{ at } 15\,\mathrm{m\,s^{-1}} \tag{4.2}$$

which is the speed estimated for the tightest corners in the competition [4]. Thereto, the wanted airfoil should have soft stall characteristics, and be very resilient to laminar separation bubbles (LSB for short. The interested

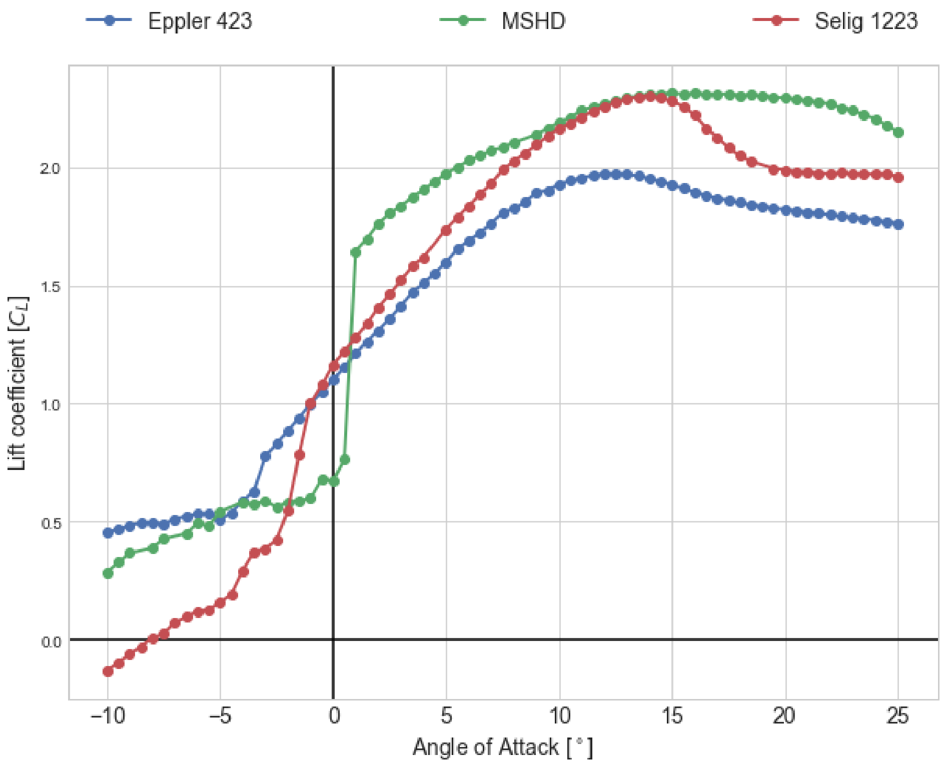

Figure 4.1: A comparison of the three airfoils as a function of angle of attack. The MSHD profile shows high lifting characteristics over a wide range of angles of attack. Comparisons are from XFOIL at $\mathrm{Re} = 3 \times 10^5$.

reader is refered to reference [2]). This is done by having a large leading edge radius.

After a thorough research comparing high lift-low Reynolds number airfoils functioning over a wide variety of angles of attack, three airfoil are selected for further examination. The Eppler E423, the Motor Sport High Downforce (MSHD) and finally the Selig S1223. The lift coefficient can be seen as a function of angle of attack in figure 4.1.

The MSHD performs incredibly well over a wide range of AOAs, with very low variation in lift coefficients. The MSHD airfoil is designed specifically for the Formula Student competition, which does make the choice rather obvious. The MSHD is selected for further investigation, and will be the airfoil of choice.

Lastly, finding the right amount of elements depends on the airfoil, and based on the MSHD profile and previous studies, two elements were chosen: A main element and a scaled down flap with 35% of the length of the main element [13]. The two elements will have an identical airfoil, as this is a classical way of generating successful multi element wings [14].

This makes production time shorter, monetary cost lower and (hopefully) provides ample lift for the first generation race car.

4.2 Dimensional Requirements

The formula student competition has a clear ruleset dictating the dimensional requirements of aerodynamic devices. The most crucial elements are outlined below:

Height Restrictions:

T7.3.1 All aerodynamic devices rearward of a vertical plane through the rearmost portion of the front face of the driver head restraint support, excluding any padding, set to its most rearward position must be lower than 1.2 m from the ground.

Width Restrictions:

T7.3.2 All aerodynamic devices higher than 500 mm from the ground, must not extend outboard of the most inboard point of the rear wheel/tire.

Length Restrictions:

T7.3.3 All aerodynamic devices must not extend further rearward than 250 mm from the rearmost part of the rear tires

Minimum Edge Radii of Aerodynamic Devices:

T7.4 All forward facing edges of aerodynamic devices that could contact a pedestrian must have a minimum radius of 5 mmfor all horizontal edges and 3 mm for vertical edges.

Rules from Formula Student UK 2018 ruleset [4].

The dimensional requirements from the rules was sketched on the front plane of the car's CAD drawing. This allows positioning the wing in the square seen in figure 4.2.

4.3 Product Design Specification (PDS)

The PDS is a design tool created to ensure that the project solves the problems it set out to. The specifications uncovered in the previous sections are boiled down to their bare essentials, and in order to cover as large a solution space as possible, the PDS contains as few *requirements* as possible. However, fulfilling the requirements is essential for a proper solution. While the criteria are not crucial, the criteria are the difference between an acceptable solution and a good one. The PDS will be revised at the discussion section, in order to verify the design solution fulfills all requirements.

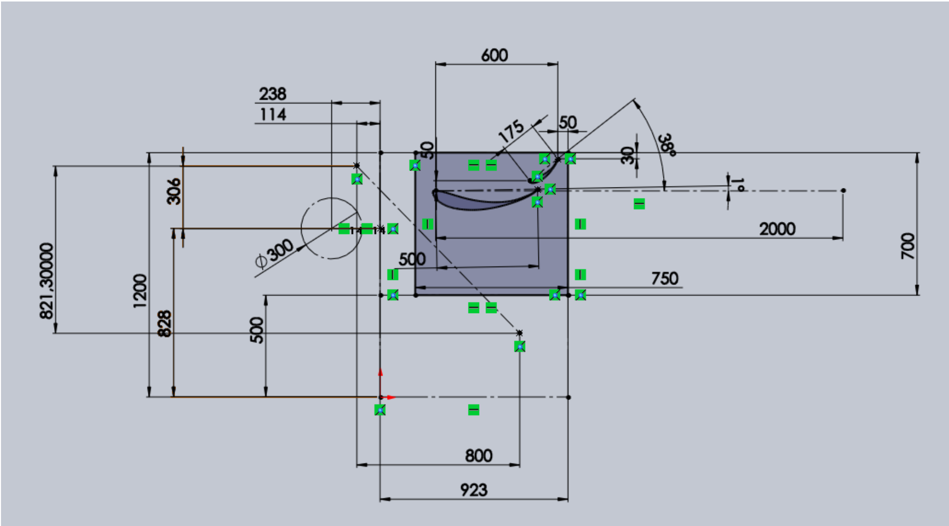

Figure 4.2: The ruleset above drawn against the design of the car. The marked square is the area where the wing can be freely placed.

Issue	Requirement	Criteria
Weight	Must not move CM above halfway point	As low as possible
Safety	Must be in compliance with FSAE rules	Should not make handling difficult for driver
Durability	Must have no fatigue limit. Must to be waterproof	
Performance	High downforce & soft stall characteristic at all speeds	Should retain perfomance despite tripping. Should have end plates.
Dimensioning	Must be within area defined by FSAE rules	Should allow space for motor removal.
Production	Low time- and monetary cost	

4.4 Initial Design

An initial design can be made based on the PDS and the design ideas above. The MSHD airfoil has a lot of the wanted characteristics: High downforce, both leading- and trailing edge stalls are soft, and the usable AOA-ranges are high. Furthermore, based on equation 3.10, we want as

Figure 4.3: Initial design of the rear wing based on the PDS and initial research. Optimization of the wing is the next step.

large end plates as possible, which will therefore fill the entirety of the allowed area. The dimensional restrictions from the competition are shown in figure 4.2. Finally, two elements are chosen as that gives a large amount of lift over even higher angles of attack, while being cheap timewise to construct.

A first draft of the design can be seen in 4.3. As the wing is intended to be optimized, a few initial assumptions were made. The first element's tail is angled 1° below horizontal, and the angle between the two wing elements is 36° based on a previous study [13]. The same article provides a first guess of the relative size of the two elements, which should be a good start for the optimization process.

4.5 Optimization Tools

In order to optimize a design, there is three ways usually employed in aerodynamics.

Road testing might seem the easiest method of testing, but constructing full-scale rear wing and iterating is very time consuming. Furthermore, in order to measure downforce correctly, suspension vibration, varying weather and such have to be taken into account, and as is the first car that's being produced, there is no car to test on. Lastly, the driver performance is rarely repeatable, thus making actual road testing a time consuming and inaccurate method of testing the wings.

Wind tunnels is another option. This allows for construction of down-scaled models, as long as Reynolds numbers are scaled accordingly. However, models can also be difficult to produce, and might not reproduce full scale results correctly. Full scale testing is expensive and wind tunnels of that size are rare.

Lastly, computational fluid dynamics offer a method of testing a wing without actually producing anything physically. Albeit the seemingly great possibilities, computer time is also expensive, and high resolution solutions require very powerful computers [2]. Luckily for us, we have access to the Niflheim7 Linux supercomputer cluster located at the Department of Physics at the Technical University of Denmark. The supercomputer has a total of 11368 CPU cores, with 235 Teraflops of processing power.

In order to verify the numerical models applied to the problem, a wind tunnel test will be performed on a 1/4 scale model and be compared to simulations. Post verification, numerical optimization of the wing will follow in Star-CCM+.

5

Wind Tunnel Experiment

Verifying the simulated aerodynamic effects is crucial to ensuring the correctness of the numerical analysis. In order to assess the reliability of the previouisly conducted simulations, a physical measurement of the pressure along the down-scaled wing will provide results for comparison. FiXme Note: sounds awful. fix

Measurements and tests have been carried out at the DTU Wind laboratory's Red wind tunnel with the help of our supervisor Robert Flemming Mikkelsen the 19$^{\text{th}}$ to the 20$^{\text{th}}$ of June.

5.1 Aerodynamical Theory

The theories explaining how fluid effects scale between varying wing sizes is explained, in order to justify using a down-scaled model as evaluation to a real size wing.

5.1.1 Similarity of Flows

In order to perform tests on the rear wing, it has to be scaled down to fit inside the wind tunnel. This reduces the physical size of the wing, which under equal circumstances changes the flow around it. In order to correctly emulate the simulated flow inside a wind tunnel, the Reynolds number and Euler number have to be the same, assuming incompressible flows:

$$\mathrm{Re}_\mathrm{m} = \mathrm{Re} \tag{5.1}$$

$$\mathrm{Eu}_\mathrm{m} = \mathrm{Eu} \tag{5.2}$$

Mathematically, the Reynolds- and Euler number are defined as:

$$\mathrm{Eu} = \frac{p_u - p_d}{pv^2} \tag{5.3}$$

where v is the characteristic velocity of the flow, p_u denotes upstream pressure, and p_d denotes downstream pressure, and:

$$\mathrm{Re} = \frac{uL}{\nu} \tag{5.4}$$

where u is the velocity relative to the object, L is the characteristic length and ν is the kinematic viscosity of the fluid.

For a down-scaled model, matching Reynolds- and Euler number requires an increase in velocity, inversely proportional to the increase in length

FiXme Note: skriv det her ud plx.

$$\begin{aligned} \frac{u_\mathrm{m} L_\mathrm{m}}{\nu} &= \frac{uL}{\nu} \\ \Rightarrow u_\mathrm{m} &= \frac{L}{L_\mathrm{m}} u \end{aligned} \tag{5.5}$$

Given the nature of the competition, the average cornering speeds are around $55\,\mathrm{km\,h^{-1}} = 15.28\,\mathrm{m\,s^{-1}}$, which is where downforce is of most importance. As shown in section 5.1.1, the desired velocity in the wind tunnel for the scale model can be found from equation 5.5

$$u_\mathrm{m} = \frac{0.6\,\mathrm{m}}{0.15\,\mathrm{m}} 15.28\,\mathrm{m\,s^{-1}} = 61.12\,\mathrm{m\,s^{-1}}$$

Which in accordance to the range of The Red wind tunnel.

5.2 Equipment

The equipment required for performing a wind tunnel test can be seen below:

- The Red wind tunnel ($60\,\mathrm{m\,s^{-1}}$ to $65\,\mathrm{m\,s^{-1}}$)
- 1/4 scale wing
- Syringe inserts
- Rubber tubing
- Pressure transducer

The instrumentation and the Red wind tunnel is described below, along with a thorough description of the scale wing designed and produced for the experiment.

5.2.1 Instrumentation

Instrumentation to perform the experiments were graciously provided to us by DTU Wind Energy. The following contains a description of the wind tunnel, datalogging devices and software used to perform the measurements.

Figure 5.1: Robert Mikkelsen posing in front of the Red wind tunnel. To the left is the air inlet, followed by the test section.

The Red Wind Tunnel

The red wind tunnel is an open loop wind tunnel located at DTU Lyngby. A picture of the wind tunnel with our supervisor Robert Mikkelsen can be seen in figure 5.1. It measures $0.5\,\mathrm{m} \times 0.5\,\mathrm{m} \times 1.3\,\mathrm{m}$ in the test section, with a maximum wind speed of $65\,\mathrm{m\,s^{-1}}$. The wind tunnel functions in low Reynolds number, which fits with the chosen MSHD aerofoil.

Pressure Measurements

The Red wind tunnel is equipped with data logging equipment measuring up to 64 pressure probes on a wing profile, the Angle of Attack (AOA), a force gauge measuring the lift forces, a pitot rake measuring the pressure in the wing's wake, the dynamic pressure in the wind tunnel, the operational speed of the wind tunnel, the air density and the time of measurement. The measurement equipment was connected to a connected to the data-logging software LabVIEW on a nearby computer.

FiXme Note: unsure here. Check document

5.2.2 Manufacturing the 1/4 Scale Rear Wing

FiXme Note: maybe fix blueprint to be more sexy/english

After the initial analysis of airfoils, this design was chosen based on preliminary research. From CITE SOMETHING HERE , a rule of thumb

FiXme Note: Insert source

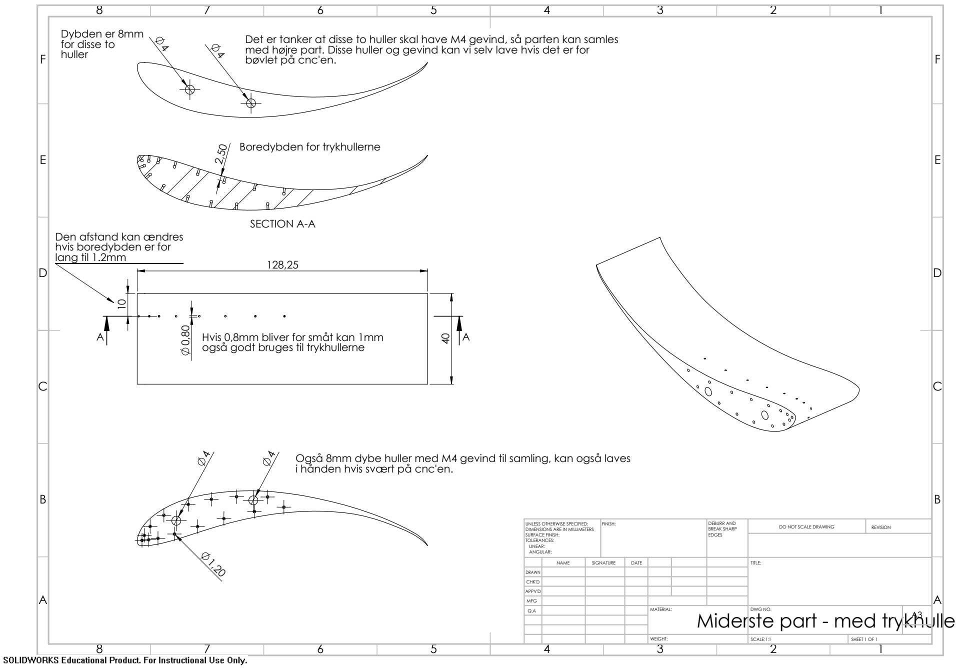

Figure 5.2: Blueprints of the centerpiece of the wing containing the pressure taps for generating a pressure distribution profile.

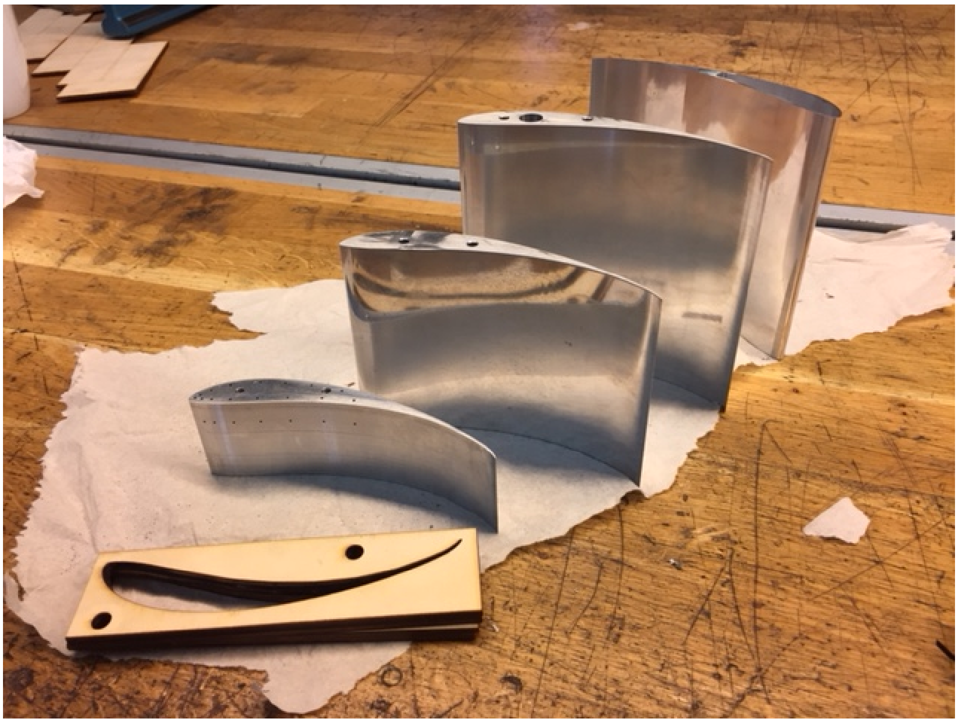

Figure 5.3: Pieces of the downscaled wing before assembly. Additional H7 holes had to be drilled in order to mount the wing to the force gauge securely.

for multi element design is that the first element should be around 70% of the total chord length, and the second element around 30%. From [2], the initial position of the elements was chosen. Having the perfect position is not essential, as the experiment is a simply a verification method of the computational method, which will be used to optimize the final deisng.

The 1/4 scale rear wing was machined at Philips Lighting by Rasmus Himborg based on the technical drawings presented below.

Blueprints

The wing requires a series of special holes for the measurements needed. 15 holes have to be made along the very narrow wing profile, in order to measure the pressure on the wing's surface. The pressure taps have to be $\varnothing 0.8$ mm on the outside, with an inner bore hole with $\varnothing 1.2$ mm, in order to have a syringe inserted. Secondly, the wing needs to be separated into smaller parts, as drilling pressure outlets through the entire wing is very difficult. Thus, the large wing is dissected into three parts. Two regular wings, and a central part with 15 pressure taps. The middle section contains the pressure outlets, where syringes serves as a connectors to rubber pressure tubes, which has to be lead out through the center of the wings adjacent of the pressure-measuring wing. Furthermore, aligning the three wing sections has to be fairly accurate. The center wing thus carries threaded holes, and the adjacent wings has M4 holes where a threaded rod can pass through and be tightened. The final design of the centerpiece can be seen in figure 5.2.

Material selection is based on the ease of machinability - a CNC-miller was provided to us, along with ample amounts of aluminium. This scale wing is not to be used in the actual race car, so weight is not a concern. Construction the 1/4 scale wing is not completely trivial. High precision is required for the surface finish, and the pressure taps have to be small in diameter: $\varnothing 0.8$ mm.

The manufactured parts can be seen in 5.3, taken shortly after receiving the parts back from Rasmus Himborg. The width of the centerpiece is based around the fact that potential upstream interference from misalignment of the wing profile sections would not cause issues around the pressure taps.

3D-printed parts

Due to machining cost and production time, the second element was 3D-printed on Zortrax M200 3D printers at DTU Skylab. the two 3d printed parts were glued together using instant glue.

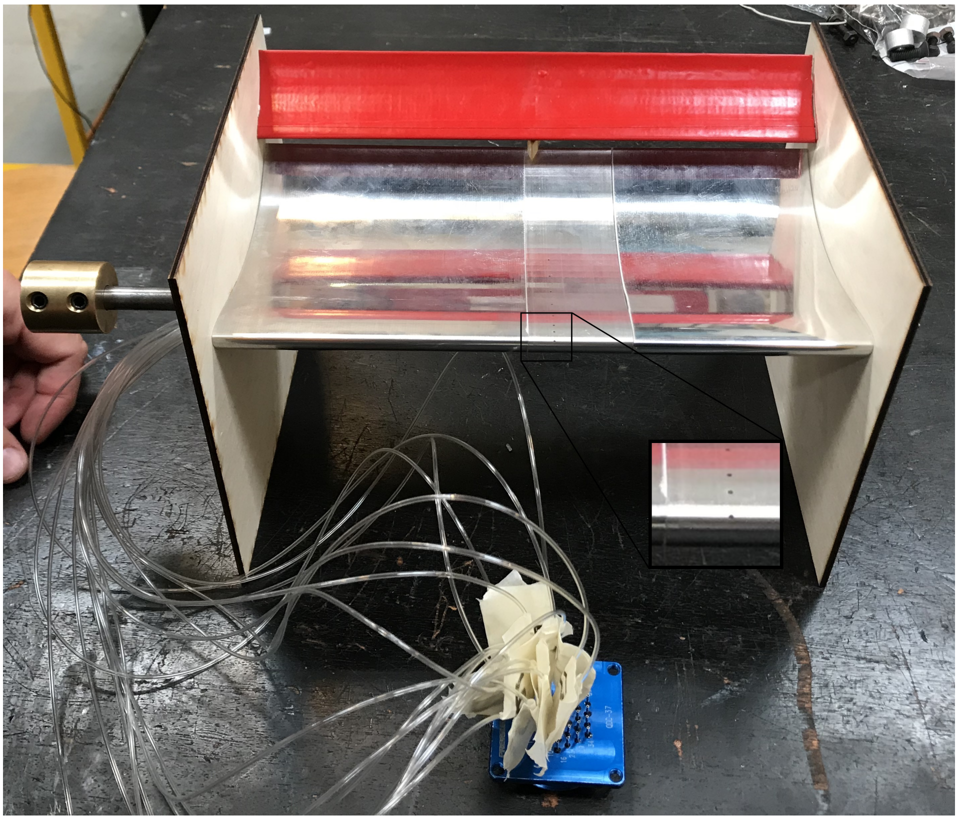

Figure 5.4: Down-scaled wing assmembled with a zoom in on the pressure taps. The length of the entire wing is approximately 250 mm with a total chord length of 150 mm.

Assembly

In figure 5.4 the down-scaled wing post-production with pressure tubes inserted can be seen with pressure-taps along the centerpiece. The wing is assembled by lasercutting the two end plates with holes for mounting, as well as the H7 mounting hole and exits for the pressure tubes.

In order to strengthen the construction and smoothen the surface, the 3D-printed rearwing was reinforced using tape. The tape is red (as seen in figure 5.4), and is additionally supported by a wooden centerpiece holding the two wings together at the right distance. Lastly, the small wing is reinforced further by attaching screws through the end plate, ensuring the wing does not flex.

5.3 Experimental Procedure

The model wing's ⌀8 mm hole is fitted with a rod at the end as seen to the left in figure 5.4, which is then mounted to the force gauge at he bottom of the wind tunnel. It is important the wing is placed as close to true level, in order to not get a skewed angle of attack initially [15]. The pressure measurement tubes are passed through a hole in the bottom of the test section, and the pressure rake's height is adjusted to measure the wing's wake. Connection is established to the LabVIEW software running on a nearby computer. A picture of the data collection UI can be found in appendix

The wing is positioned with a $0°$ angle of attack. Measurements are taken with $10\,\mathrm{m\,s^{-1}}$ increments in the range of $10\,\mathrm{m\,s^{-1}}$ to $60\,\mathrm{m\,s^{-1}}$, with an angular sweep at $20\,\mathrm{m\,s^{-1}}$ and $40\,\mathrm{m\,s^{-1}}$, in order to compare the optimum angle of attack with litterature.

However, due to the wing covering a relatively large area of the wind tunnel, the final test could only go to $59.2\,\mathrm{m\,s^{-1}}$.

FiXme Note: what's the level of obstruction?

5.4 Results

The results from the experiment is divided into two parts: A comparison with the theoretical lift values of the downscaled wing, and a comparison with the simulated results. The simulated results will be shown in section 6.4.1, while the comparison to theory can be seen in this section.

The theoretical lift coefficient at of the scale wing using a total AOA of $\alpha = 35°$, an effective additional AOA from the wing's camber of $\alpha_{L_0} = 0°$ CITE SOMETHING HERE and equation 3.3 is found to be:

$$C_L = \left(\frac{2\pi}{1 + \frac{2}{\frac{b}{c}\left(1+1.9\frac{h}{b}\right)}} \right) (\alpha + \alpha_{L_0})$$

$$\Rightarrow \left(\frac{2\pi}{1 + \frac{2}{\frac{250\,\mathrm{mm}}{155\,\mathrm{mm}}\left(1+1.9\frac{175\,\mathrm{mm}}{250\,\mathrm{mm}}\right)}} \right) \left(\frac{35\pi}{180} \right) = 2.51$$

Comparing the theoretical lift to the lift coefficients found by the experiments is seen in figure 5.5. The purple line is the theoretical lift, where the wing's angle is swept between $-10°$ and $10°$. The measured lift is slightly lower than the theoretical, which may be explained by the end plate's effect on aspect ratio. The downscaled wing has a very large Æ, where the end plates extend far below the bottom of the wing. While theoretically positive, the effect of the long end plates might not extend all the way up to the wing profile, artificially inflating up the theoretical lift number.

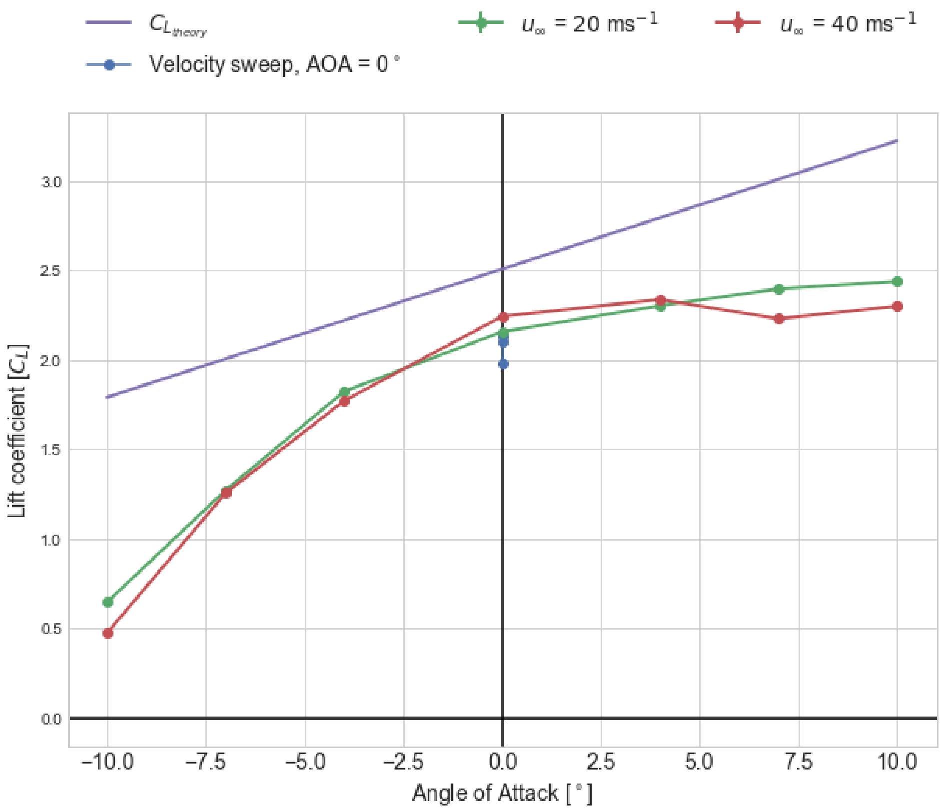

Figure 5.5: The lift coefficient plotted as a function of the wing's overall AOA. The wing's own angle of attack is 35°, which is beyond the theoretical optimum as seen in figure 4.1.

6

Simulation

The simulation will run in several parts. First, the wings relative placement between eachother will be optimized in a 2-dimensional environment. This involves, size, x- and y-distance between the multi-element wings, angle of attack and height relative to the chassis to give a good estimate of the wings placement range. Secondly, a 3-dimensional analysis of the entire wing with endplates will be performed. Endplate dimensions will be optimized, and further optimization of the height relative to the entire chassis to finalize the design and placement. Lastly, a complete computational solution to the entire car will finalize the aerodynamical package, and yield the total amount of drag and downforce.

6.1 Star-CCM+

Star-CCM+ was used to run the simulations of the wing first in the wind-tunnel for verification and next on a model of the full size wing to produce an estimate of the performance at full scale. As meshing and running the simulations were heavy computational tasks, the computations were run on the *Niflheim Linux cluster supercomputer*, which is installed at the Department of Physics at DTU.

6.2 Finite Volume method

Star-CCM+ employs the finite volume method, which will be covered briefly in this report.

6.3 Mesh Generation

««««< HEAD The mesh has to be structured in accordance to best practice. Areas with high velocity and pressure gradiants have to be dissolved in acceptable resolutions, in order to ensure correct results. Running an initial test on a generic mesh shows us where the wing requires greater resolution. Gradiants are easily visible around the wing's leading edge, and generally around the solid bodies. Furthermore, aligning the meshg with the flow improves accuracy and rate of convergence. .

FiXme Note: Noget med konvergens undersøgelse. Måske også grid sensitivity test.

Generating a mesh of correct size is done by sampling downforce over a range of mesh sizes. In figure **??**, the downforce plotted as a function of the mesh size shows a tendency towards 125 N for the downscaled wing. The function converges to acceptable levels near the mesh size 4×10^6, and serves to be a good compromise ======= The mesh has to be structured in accordance to best practice. Areas with high velocity and pressure gradiants have to be dissolved in acceptable resolutions, in order to ensure correct results. Running an initial test on a generic mesh made it clear where the volumemesh requires greater resolution. Gradiants are easily visible around the wing's leading edge, and generally around the solid bodies. Furthermore, aligning the mesh with the flow improves accuracy and rate of convergence. To determine the convergence of simulation results six different mesh resolutions where used to examine the simulations for the windtunnel setup with a wind velocity of $40\,\mathrm{m\,s^{-1}}$. Finding the minimum mesh resolution where results have converged with higer resolution results, means a minimum computation time can be achived and thereby allowing for more simulations to be run. »»»> f095ae55e7c166f37a89e1954bd718f58d7b7784

6.4 Optimizing the Rear Wing

6.4.1 Verification of Simulation Results

Comparison with wind tunnel test.

Evaluation of Verification Simulation

6.4.2 Multi-Element Wing Optimization

The influence of the two wing elements relative position on lift was examined to optimize the downforce the rear wing provides to the car at a given velocity. This relative position optimization was performed in the software package *MultiElements Airfoils* provided from *Hanley Innovations*. A scatterplot of the relative position is seen in figure 6.4.2. The trailing

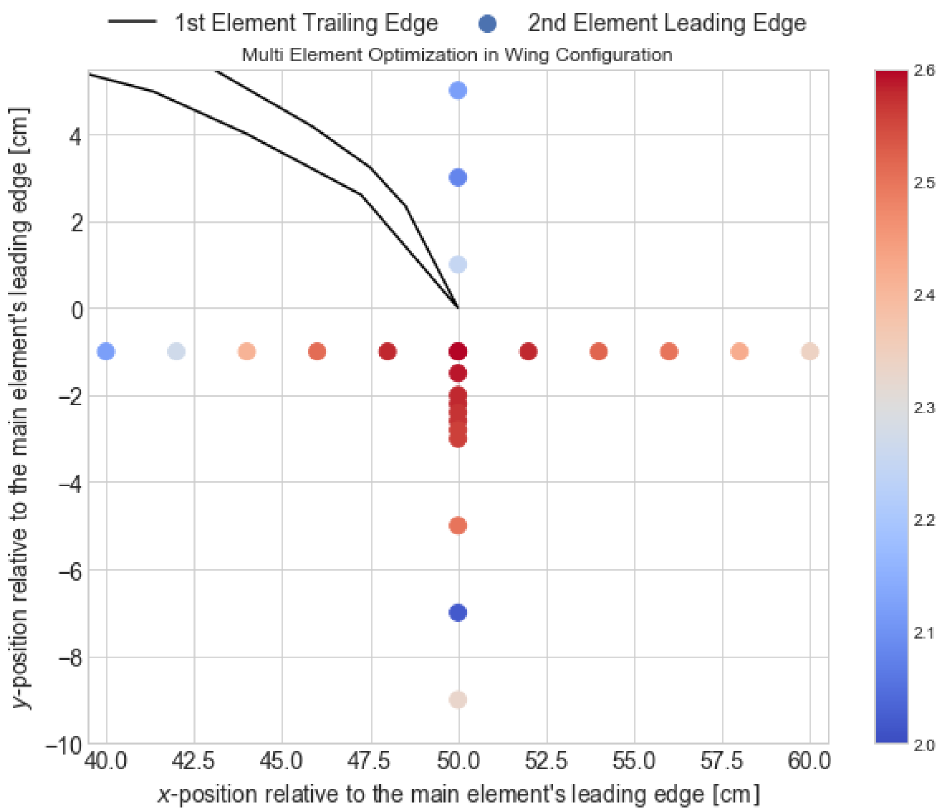

Figure 6.1: Optimization of the two element wing. The redder the dots, the higher the lift coefficient.

edge of the first element is seem as the dark lines, and the position of the second elements leading edge is plotted, where the resulting lift coefficient is embedded as color. The redder the better lift coefficient. After sweeping, a maximum lift of $C_L = 2.60$ at $u = 15\,\mathrm{m\,s^{-1}}$. is found with the leading edge of the secondary element placed at $x = 0.5\,\mathrm{m}, y = -0.01\,\mathrm{m}$ relative to the leading edge of the main element.

6.5 Results

7

Construction

This chapter concerns the construction of the rear wing. The step from theoretical abstraction to a real product. This includes dimensioning, material selection and finalizing the design. The simulated rear wing lacks a proper mounting method design, which is also included in this chapter.

7.1 Requirements

The formula student competition has a clear ruleset dictating the strength requirements of aerodynamic devices. The most crucial elements are outlined below:

7.1.1 Strength Requirements

Aerodynamic Devices Stability and Strength:

T7.5.1 Any aerodynamic device must be able to withstand a force of 200 N distributed over a minimum surface of 225 cm^2 and not deflect more than 10 mm in the load carrying direction.

T7.5.2 Any aerodynamic device must be able to withstand a force of 50 N applied in any direction at any point and not deflect more than 25 mm.

Rules from Formula Student UK 2018 ruleset [4].

This constraint give us an allowed elastic modulus of:

$$E \equiv \frac{F/A}{\Delta L/L_0} \Rightarrow \qquad \frac{200\,\text{N}/225\,\text{cm}^2}{3\,\text{mm}/10\,\text{mm}} \tag{7.1}$$

As the wing will be mounted against the end plates, it can be considered a simply supported beam. The elastic deflection is thus described by:

$$u = \frac{FL^3}{48EI} \quad (7.2)$$

where u is the deflection at the midpoint, F is the force applied, L is the length of the beam (the same as b for wings), E is the elastic modulus of the wing and I is the moment of inertia of the cross section.

7.2 Material Selection

Selecting a fitting material depends on the maximum deformation and weight. According to the PDS (see section 4.3), the wing has to be *as light as possible* in order not to move the center of mass further upwards. Furthermore, it needs a high *elastic modulus* in order to be stiff as to not deform by aerodynamic forces. The wing needs to be have a *high yield strength*, be *low cost* and easy to produce time wise.

Drawing on experience from competitors, carbon fiber- and glass fiber reinforced polymers are the weapons of choice [16]. However, Cambridge Engineering Selector, a material selection tool was used in order not to leave a stone unturned. The results can be seen in figure 7.1, where the highly tensile strong materials are plotted against their density. Magnesium and some aluminium alloys are near the carbon fiber reinforced polymers, but machining an entire wing out of metal is incredibly time consuming and expensive. Carbon fiber reinforced polymers are chosen as a material, and the next chapter will investigate the properties and strength of the composite structure.

7.3 Composites

The strength of composites come from the fiber.

7.3.1 Sandwich Structure

The bending stiffness for a simple sandwich panel

7.3.2 Wing Deflection

7.4 Final Design of Rear Wing

FiXme Note: Presentation of CAD Drawings and method of how we will get to this result

FiXme Note: Rendering

The two elements of the full scale wing will be bolted to the endplates at the optimal found angle of attack. The wing elements will have two metal

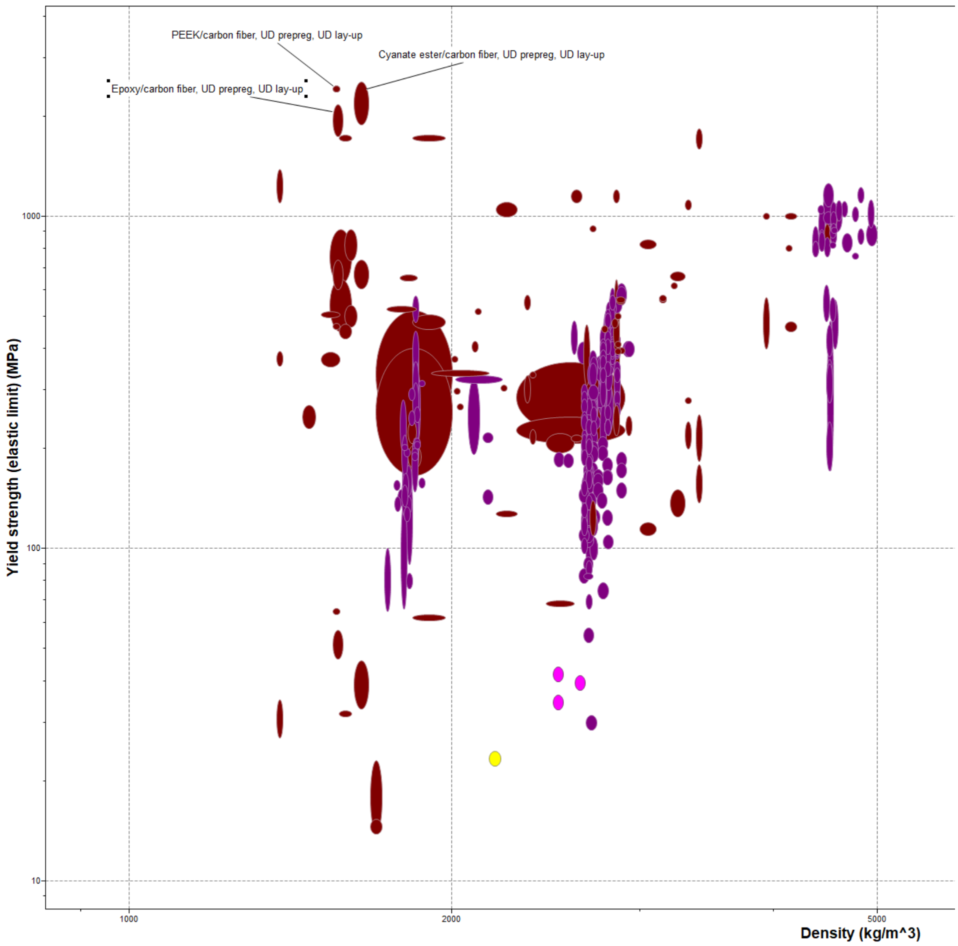

Figure 7.1: Cambridge Engineering Selector (CES) showing the various aerospace grade materials usable for this application. The dark red dots are compositites, while the dark purple dots are metals such as aluminium and magnesium.

brackets glued to the inside of the carbon fiber wings, the bracket will be have holes with M10 threads in which the endplates are bolted to secure the structure.

7.4.1 Topology Optimization

In order to minimise the weight of the metal bracket inserts topology optimizations where made using the build in function in *Fusion 360*, in which all simulations are done in the cloud. Topology optimization tries to reduce the weight of the model by removing excess material while maintaining stiffness and strength of the model. The inserts were modeled from the wing profile and the location of the inner threads was chosen. The model was then meshed with a target cell size of 1.5 mm, and the

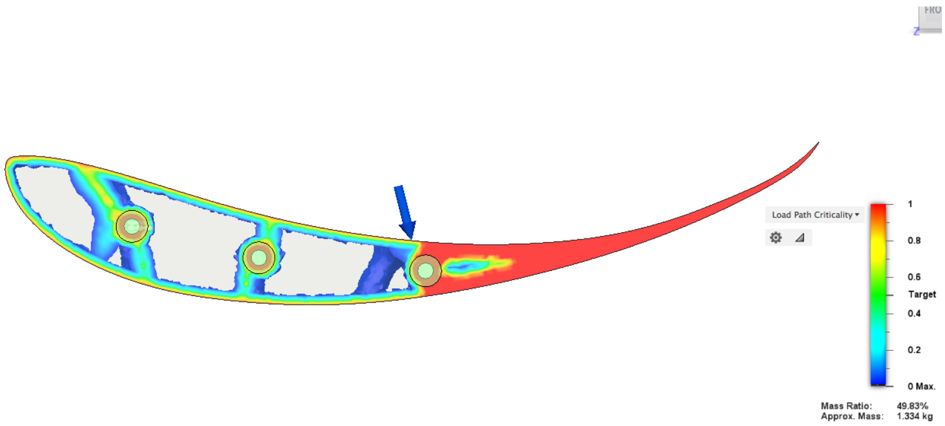

Figure 7.2: The result of the topology optimization for the large insert, with a weight reduction at about 50 %.

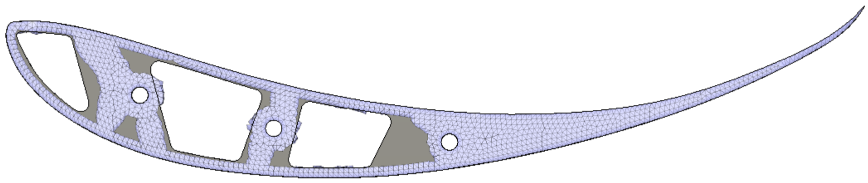

Figure 7.3: Optimized mesh overlayed on model so excess material could be easily removed.

target weight reduction was set to 70%, with a downforce load of 250 N at the surface.

The result of the optimization for the large insert is shown in figure 7.2, was then used to remove excess material from the model. The results were overlayed on the model and material could be cut from the original model as shown in figure 7.3. The final model of the large insert was then created with a weight reduction around 40 %. A render of the final model is shown in figure 7.4. The same procedure was done for the smaller metal wing insert, and technical drawings of are included in following section.

The two elements of the full scale wing will be bolted to the end plates at optimal found angle of attack. The wing elements will have two metal brackets glued to the inside of the carbon fiber, the bracket will be have holes with M10 threads in which the endplates are bolted to secure the structure.

Figure 7.4: Render of the final model for the metal insert, with a weight reduction around 40 %.

7.4.2 Blue Prints

7.5 Manufacturing Final Design

The following section describes the steps required to build the wing physically. First, templates of the MSHD airfoil are lasercut. The templates are mounted on the sides of polystyrene blocks, where a homemade hot wire cutter cuts the foam cores of the wing. The foam cores are then glued together into the appropriate lengths, where the carbon fiber mattes are draped over. The carbon fiber is then reinforced by an epoxy resin, which over a 24 hour period is hardened. The surface is then polished, and finally resealed by adding another layer of epoxy resin. The wing is then bolted to the end plates through the two metal brackets inserted into the wing ends. Lastly, brackets for mounting the wing on the chassis are inserted, where the potential buckling of the rods is accounted for.

7.5.1 Polystyrene Molds

The molds for the wings were chosen as positive molds, meaning polystyrene molds of the actual wings were cut out and overlaid with resin coated carbon fiber. In order to do this, we devised a hotwire-based specialized tool for the job. This can be seen in figure 7.5, where a gauge 4 wire was used at 12 V drawing 2.5 A over a cutting length of 600 mm. In order to get the correct airfoil shapes, the MSHD airfoil profile was lasercut out of 3mm plywood. The wooden profile is then mounted on the sides of the polystyrene block, where the hotwire is pulled across in a timely fashion. In order to produce a smooth surface, two people have to move very coordinated. Going too slow leaves deep melting lines, and moving too fast lets the hotwire ”slack” in the middle because it does not melt the polystyrene quick enough, which causes the airfoil profile to be skewed.

All hotwire cutting was done by hand over several days, and we owe a

Figure 7.5: The hot wire melts the styrofoam while sliding along the wooden template.

Figure 7.6: Steffan and Nicolai performing a hand layup of the carbon fiber mats around a polystyrene foam core.

special thanks to our sponsor DTU Skylab for providing the polystyrene blocks.

7.5.2 Hand Layup

The data sheet of the carbon fiber weave can be found in appendix B, the hardener used can be found in appendix C and the resin used can be found in appendix D.

The finished positive molds are used both as molds where carbon fiber is applied on, as well as foam cores that reinforce the structure. The molds are then placed inside the negative forms of the molds, where carbon fiber is draped over the surface. The epoxy is then applied to the carbon fiber matte by a soft brush, and air is rolled out by spiked rollers. Nicolai Boertman is seen performing this action in figure 7.6, putting the final layer on the main element of the rear wing. The white polystyrene mold underneath the carbon fiber is the negative mold, which helps keep the shape when applying to carbon fiber to the other side. After rolling out the epoxy satisfyingly, a plastic tarp is added to the surface and rolled down neatly without air bubbles. This ensures getting a smooth surface, and lets the wing cure occur in a closed environment.

Three methods of curing was attempted:

Figure 7.7: Curing the wing in a flat position let the resin pool in the center of the wing, making the surface very rough.

The wing hanging freely with no pressure: The results was good. No pooling of epoxy, the surface was relatively smooth, but an additional sealing layer had to be applied, as the epoxy had been displaced from the surface. This gave it the surface roughness of the fibers, which is not optimal. The wing laying flat under pressure with the convex shape pointing upwards: This was highly successful, giving a very smooth surface with the right amount of epoxy covering it. No additional treatment was required. The concave shape pointing upwards: The results was not good, but workable. The results can be seen in figure 7.7. The epoxy pooled due to gravity forcing the epoxy down towards the center of the cambered wing. Getting a proper surface finish from this is handled in the section below.

7.5.3 Surface Finish

Curing *should* occur by securing the wing *vertically* or with the convex shape pointing upwards, as to not let epoxy pool up on the concave surfaces. This knowledge was forgotten on one of the wings, as seen in figure 7.7, where the surface has become very rough due to epoxy pooling.

Figure 7.8: Sanding the wing clears the surface roughness, but requires a new layer of sealant. Using epoxy or a lacquer was investigated before settling on epoxy.

Albeit not optimal, the wing can be salvaged by sanding.

7.5.4 Implementation and Testing

7.6 Testing and Inspection

7.6.1 Reinforcing the mounting

8

Discussion

8.1 Product Design Specification Review

The finished product have to live up to the design specification, in order to be a useful solution. In table 8.1, it can be seen that all reqirements are fulfilled, and all criteria except one. During the design process of the car, the removal of the engine became negligible as the battery pack is going to be removed in another way. This voids the criteria, and thus makes the solution an optimal one.

Issue	Requirement	Criteria
Weight	Must not move CM above halfway point	Should be as low as possible
Safety	Must be in compliance with FSAE rules	Should not make handling difficult for driver
Durability	Must have no fatigue limit. Must to be waterproof	
Performance	High downforce & soft stall characteristic at all speeds	Should retain perfomance despite tripping. Should have end plates.
Dimensioning	Must be within area defined by FSAE rules	Should allow space for motor removal.
Production	Low time- and monetary cost	

Table 8.1: The PDS table shows how the final design lives up to the proposed specifications.

9

Conclusion

bla

Perspective

The Eevee has to be rebuilt next year, and in order to help the effort along for future students, a list of potential upgrades are listed below, with estimates of how valuable each change is in regards to downforce/drag reduction gain.

9.1 Drag Reductive System

A drag reductive system (DRS) is well-known from Formula 1, and has in the recent years been gaining traction (or lack therof :)))) in the Formula Student. It is a natural extension to the aerodynamics of the car, as Formula Student has much less restrictions on aerodynamics than Formula 1. Automatically adaptive DRS, that measures the car's relative downforce and the angle of the steering column could give a big edge on straights, as flipping the wing up to reduce drag increases the top speed.

9.2 Slats, Flaps, Gills and Cutaway

https://www.jmranalytical.com/single-post/2017/04/06/Rear-Wing-Investigation

We already have a multi element wing, but increasing the amount of elements increases the amount of downforce we can pull out of the same design.

9.3 Suspension Integration

- Nice to have downforce directly on the wheels - Gives more unsprung mass though. That might be an issue.

Media

The project gained a lot of media attraction. For the interested reader, more can be found below.

A

Appendix

A.1 Appendix A

Figure A.1: qed

B

Carbon Fiber Data Sheet

C

Hardener Data Sheet

D

Resin Data Sheet

Bibliography

[1] Bulbapedia. http://bulbapedia.bulbagarden.net/wiki/Eevee, may 2016.

[2] Joseph Katz. *Race Car Aerodynamics*. BentleyPublishers, 2nd edition, 2003.

[3] J.R. Taylor. *Classical Mechanics*. University Science Books, 2005.

[4] IMechE: Institution of Mechanical Engineers. *Formula Student Rules*. 2018.

[5] lcdesign. Formula sae aerodynamics. https://sites.google.com/site/lcdesignwork/case-studies/automotive-case-studies/formula-sae.

[6] HPWizard. Tire friction and rolling resistance coefficients. http://hpwizard.com/tire-friction-coefficient.html.

[7] Hucho W. *Aerodynamics of road vehicles*. Warrendale, 4th edition, 1998.

[8] NASA. The lift coefficient. https://www.grc.nasa.gov/www/K-12/airplane/liftco.html.

[9] NASA. The lift coefficient. https://www.grc.nasa.gov/www/K-12/airplane/dragco.html.

[10] NASA. Induced drag coefficient. https://www.grc.nasa.gov/www/k-12/airplane/induced.html.

[11] NASA Langley Research Center. Vortex created by the passage of an aircraft wing. https://en.wikipedia.org/wiki/Vortex#/media/File:Airplane_vortex_edit.jpg.

[12] Peter Kämpf. Lift creation and induced drag. https://aviation.stackexchange.com/questions/8556/is-a-winglet-better-than-an-equal-span-extension/8579#8579.

[13] P.S. Sriram, Ashok Gopalarathnam, and Andrew Misenheimer. High-downforce airfoil design for motorsports, 2012.

[14] R.H. Barnard. *Road Vehicle Aerodynamic Design: An Introduction*. MechAero, 2001.

[15] Dan Harmon Justin Roiland. `https://youtu.be/w-wbWGwZ7_k?t=43s`, 2017.

[16] G Savage. Composite materials technology in formula 1 motor racing. *Honda Racing F1 Team*, 91:92, 2008.